



HAL
open science

Investigating the plastic anisotropy and hardening behavior of a commercial Zn-Cu-Ti alloy: Experimental and modeling approach

Ludovic Cauvin, Balaji Raghavan, Jianqiang Jin, Salima Bouvier, Xiaodong Wang, Fodil Meraghni, Jose Luis Alves

► To cite this version:

Ludovic Cauvin, Balaji Raghavan, Jianqiang Jin, Salima Bouvier, Xiaodong Wang, et al.. Investigating the plastic anisotropy and hardening behavior of a commercial Zn-Cu-Ti alloy: Experimental and modeling approach. *Mechanics of Materials*, 2022, 164, pp.104103. 10.1016/j.mechmat.2021.104103 . hal-03464826

HAL Id: hal-03464826

<https://hal.science/hal-03464826>

Submitted on 10 Dec 2021

HAL is a multi-disciplinary open access archive for the deposit and dissemination of scientific research documents, whether they are published or not. The documents may come from teaching and research institutions in France or abroad, or from public or private research centers.

L'archive ouverte pluridisciplinaire **HAL**, est destinée au dépôt et à la diffusion de documents scientifiques de niveau recherche, publiés ou non, émanant des établissements d'enseignement et de recherche français ou étrangers, des laboratoires publics ou privés.



Distributed under a Creative Commons Attribution - NonCommercial 4.0 International License

Investigating the plastic anisotropy and hardening behavior of a commercial Zn-Cu-Ti alloy: experimental & modeling approach

Ludovic Cauvin^{a,1}, Balaji Raghavan^b, Jianqiang Jin^a, Salima Bouvier^a, Xiaodong Wang^a, Fodil Meraghni^c, José Luís Alves^d

^a *Université de Technologie de Compiègne
Roberval (Mechanics, energy and electricity), Centre de recherche Royallieu - CS 60319 -
60203 Compiègne Cedex - France*

^b *Laboratoire de Génie Civil et Génie Mécanique EA 3913, INSA de Rennes, France*

^c *Arts et Métiers ParisTech Metz, LEM3-UMR7239, F-57000, Metz, France*

^d *CT2M, Department of Mechanical Engineering, University of Minho, Campus de Azurém, 4800-058 Guimarães, Portugal*

Abstract

The aim of this work is to conduct a comprehensive examination of the anisotropic plastic behavior of a sheet of commercial Zn-Cu-Ti alloy, undergoing different quasi-static deformation paths at room temperature. Various mechanical tests are performed, including uniaxial and bi-axial tensile tests, Meuwissen and shear tests, obtaining homogeneous and heterogeneous strain fields. It was observed that under monotonic loading, the material behavior, i.e. stress evolution and ductility, is very sensitive to the loading direction. During reverse loading, the material displays a high Bauschinger effect, with behavior that is strongly dependent on the forward shear direction. For the Meuwissen-like tests, it has been found that the force-displacement curve as well as the maximum ductility are very sensitive to the in-plane anisotropy. The yield parameters are identified by direct comparison of the experimental results with classical anisotropic yield models. Finally, the plastic anisotropic behavior of the investigated zinc sheet is simulated for various mechanical tests using Finite Element Analysis to identify the related hardening parameters.

¹corresponding author: ludovic.cauvin@utc.fr

Keywords: Anisotropy, Ductility, Hardening, Heterogeneous test, Rolled zinc, ZnCuTi, FE simulations

1. Introduction

Zinc alloys rolled sheets present the advantage of aesthetic quality with excellent visual appearance, long life with minimal maintenance, reduced cost and adaptability which enable them to be widely used in a variety of civil engineering applications such as the fabrication of roofing products, cladding, flashings, rainwater down-pipes disposal applications and also for more innovative architectural designs. They also find several other uses, from electrical components to table tops, in addition to specialized applications such as in photoengraving surfaces. Because of this wide range of applications, Zinc and Zinc alloys have already found a great interest in the scientific community. But much of the published literature on rolled sheets of zinc-based alloys has focused on their corrosion resistance (e.g. [1, 2, 3, 4]). This is understandable, given that the primary application for these materials is in the field of civil engineering, where the Zn sheets are generally exposed to highly aggressive environments.

Anisotropy in metals may arise due to various reasons, for example, the earliest observation by Hill [5] of the formation of Lüders' bands in annealed mild steels that was unable to be modeled using the von Mises yield criterion. Hexagonal Close Packed (HCP) materials show significant anisotropy in their mechanical properties due to their initial marked textures, deformation mechanisms and critical shear stresses, which in turn are dependent on the activated slip systems (e.g. basal or pyramidal) as well as the sense of the applied stress (e.g. asymmetry of twin activation). Zinc and its alloys are typical metals with HCP lattice structure with a c/a ($=1.856$) ratio higher than that of an ideal structure (i.e. 1.633), on account of which they have relatively few independent slip and twinning systems [6, 7, 8].

Generally, HCP materials exhibit several types of twinning. However, for zinc based materials, deformed at isothermal or comparable temperature, twinning

along the $\{1\ 0\ -1\ 2\}$ planes is the dominant mechanism that allows for inelastic shape changes along the c-axis [9]. Since the c/a ratio for zinc-based materials is greater than the *ideal* value, the direction of shear due to twinning activation is $[1\ 0\ -1\ -1]$ [10, 11] and twinning occurs under compression parallel to the c-axis, but also under uniaxial tension along the transverse direction for split basal texture in Zn-based rolled sheets.

The earliest work on the macroscopic mechanical behavior of Zn-Cu-Ti alloy rolled sheets was by [12] in 1968, using uniaxial tensile tests along different orientations with respect to the rolling direction (RD). They estimated initial yield stresses and strain ratios and the response to biaxial loading was studied using the circular bulge test. Hill's theory of plasticity with orthotropic symmetry [5] was unable to predict the stress-strain curve under biaxial loading, hinting that the significant anisotropic behavior of these materials could not be described by this theory.

[13] examined the anisotropic plastic behavior of zinc rolled sheets at the crystallographic scale using pole figures and metallographic observations. The material was deformed using uniaxial tensile loading along the rolling and transverse directions, and the circular bulge test. The active deformation mechanisms were identified, and tensile yield stresses and strain ratios (i.e. Lankford r-values) were predicted considering slip along the identified systems according to the maximum shear stress criterion. These were in reasonable agreement with the experimental values. According to the authors, the macroscopic theory of plastic anisotropy was based on two main assumptions (at the time): variations of the strain-hardening characteristics with orientation were not taken into account, and the constitutive relation was not affected by the sign of the stress, which was known to be untrue in case of deformation twinning. This led them to conclude that the macroscopic theory of plastic anisotropy was inadequate.

[14, 15, 16] studied the microstructure and relationship between texture, composition and bendability. Kataoka et al [17] analyzed the dry deep drawability of a pure zinc sheet using ceramic tools (Alumina, Zirconia, Silicon nitride and Silicon carbide). The authors observed early cup failure when using the classical

alloyed tool steel. Conversely, they pointed out the good adaptability of zinc to ceramic dies since the LDR (ratio of maximum blank diameter to the punch diameter) was significantly promoted for such tools, with silicon nitride dies showing a greater improvement. In 2007 Pantzopoulos et al [18] investigated the effect of welding Zn-Cu-Ti rolled sheets on their failure resistance. Some other recent literature [19, 20, 21, 22, 23, 24] including our own previous work [25] has focussed on linking the evolution of the mechanical behavior and/or anisotropy with the initial microstructure.

The ever-increasing list of applications of this class of materials necessitates the development of accurate numerical simulations of their forming processes. Due to their significant anisotropy, the experimental forming set up that allows for the stamping to produce the desired (usually complex) 3D shapes is time consuming and judicious sequences of several forming steps should be achieved in order to reach the desired forms. The optimization of such sequences can be readily accomplished based on numerical simulation using suitable phenomenological models for these materials.

To the best of the authors' knowledge, relatively less attention has been given to the mechanical and macroscopic modeling of the anisotropic behavior of zinc-based alloys under several loading paths in spite of the continuing widespread use of these materials. A few papers on modeling of the anisotropic behavior of zinc alloys are based on micro-mechanical approaches.

In 1994, [26] investigated crack occurrence in bending tests by studying the microstructure and texture evolution during cold rolling of Zn-Cu-Ti alloy sheets. They used the Relaxed Constraint Taylor micro-mechanical model and compared it with results obtained using other micro-mechanical models (Sachs, Full Constraint Taylor) for the prediction of texture evolution at large rolling reduction. The authors concluded that the most important factor controlling the predicted behavior was the accuracy of the model of the physical mechanisms involved, with consistent identification of the critical shear stresses for the activated systems. Fundenberger et al [27] modeled the mechanical properties in terms of in plane initial yield strength and plastic strain ratio distribution for

Zn-Cu-Ti alloy rolled sheets. Through a reliable determination of the main active systems and the corresponding critical resolved shear stresses, the authors had succeeded in accurately predicting the texture evolution and mechanical properties using micro-mechanical models (constrained and relaxed variants of Taylor model). These models were chosen for their ability to predict the deformation mechanisms (i.e. frequency of occurrence) obtained as a result of a statistical study carried out at the optical and microscopic scales. The initial anisotropic yield surface was therefore determined in the sheet plane. Research similar to [26] for the case of asymmetric rolling was recently proposed by [28]. Our previous contribution [25] involved uniaxial tensile tests along 3 directions ($0^\circ/\text{RD}$, $45^\circ/\text{RD}$ and $90^\circ/\text{RD}$) for comparing the experimental data with the predictions of a multi-scale Visco-Plastic Self-Consistent approach [29].

The aim of the present paper is to provide the results of a comprehensive investigation of the anisotropic behavior of rolled Zn-Cu-Ti sheet under monotonic and reverse loadings at moderate strain levels using both homogeneous and heterogeneous mechanical tests. The results shown here are intended to complement those obtained on the exact same material (albeit with a different thickness of 0.65 mm) in our previous work related to micro-mechanical modeling of rolled zinc alloy sheets.

The paper is divided into six main and complementary sections. The next section presents the experimental procedure and the material description. The third section describes the experimental results, with comments and discussion. The fourth section presents the constitutive phenomenological (macroscopic) model for the material that has been adopted in this work. The fifth and sixth sections detail identification of the material yield and hardening parameters respectively along with Finite Element simulations for the stress-strain response and the initial yield surface. The paper ends with concluding comments and recommendations for future work.

2. Material and experimental techniques

In this section we describe the material being characterized along with the main experimental tests used in this work.

2.1. Material description

The present work concerns rolled sheets of a commercial Zn-Cu-Ti alloy. The chemical composition is given in Table 1 and meets the EN988:1997 standard requirements.

This alloy possesses a good balance of mechanical properties including forma-

Alloy	Cu	Ti	Al	Zn
Zn-Cu-Ti	> 0.08 < 1.0	> 0.06 < 0.2	— — — < 0.015	remainder

Table 1: Chemical composition (%m/m) of the rolled Zn-Cu-Ti commercial zinc alloy.

bility, tensile strength and creep resistance. The material is delivered in sheet form with 1 mm thickness.

From EBSD observation, the material is seen to be fully recrystallized with equi-axed grains of uniform size and the as-received material does not display any twinning.

2.2. Mechanical characterization

Mechanical characterization typically involves several mechanical tests like uniaxial/bi-axial tensile/compression tests, forward/reverse shear tests, indentation in order to identify the parameters of some chosen constitutive mechanical model.

For all the mechanical tests carried out in the present work, the reproducibility was checked by repeating them up to three times each. The mechanical tests were performed under quasi-static loading at fixed strain rate along different orientation with respect to the rolling direction (RD) in order to thoroughly examine the material in-plane anisotropy.

For all tests, several images were taken for the purpose of measuring the displacement fields using an optical device (2 megapixel cooled camera 4096 grey level, placed in front of the specimen surface) and the strain fields are calculated using digital image correlation (DIC) with VIC2D software. For the Digital Image Correlation (DIC) [30, 31, 32], the specimen was prepared by spraying a thin coat of matt black paint on its surface, followed by a white coat in order to create a speckle pattern on the gauge area. The spatial resolution of the DIC technique depends on the quality of the speckle. In this study, the pattern resolution of 32×32 pixels has been used.

2.2.1. Uniaxial tension

Tensile test specimens (figure 1) have a geometry according to the ISO 80/20 norm (80 mm length and 20 mm width in the gauge area), cut out from the as-received sheets by hyperbar water jet.

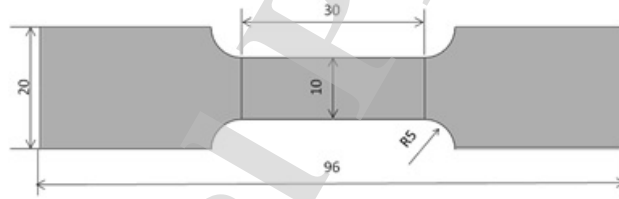


Figure 1: Uniaxial tensile test specimen according to the ISO 80/20 norm

All tensile tests have been conducted at constant true strain rate of $10^{-3} s^{-1}$ in order to guarantee that the tests are quasi-static. The uniaxial tensile tests are performed at various orientations with respect to the rolling direction, namely 0° , 15° , 30° , 45° , 60° , 75° and 90° . The deformation is controlled by a high-resolution extensometer on a rather short measuring base. Full field displacement measurements are performed in order to determine full strain distribution with the gauge area and to examine the strain anisotropy along different orientations with respect to the rolling direction over a wide range of plastic strain. The orientations 0° , 45° and 90° with respect to the rolling direction have already been studied in a previous study (for sheets with a thickness of 0.65 mm)

[25] but other orientations have been considered here to study the anisotropy of the considered Zinc alloy.

2.2.2. Simple shear

Planar simple shear testing has proved to be a very efficient technique to evaluate the mechanical properties of flat samples [33]. In contrast with the commonly used uniaxial tensile test, the simple shear test has many advantages such as simplicity of the sample geometry (e.g. rectangular shape) and the ability to achieve large homogeneous strains and rotations. Moreover, in cyclic tests the loading direction can be easily reversed during the experiment by simply changing the displacement direction of the clamps, without modifying the clamps or re-machining the sample. More details can be found in [34, 35]. All the tests were conducted at a constant and controlled equivalent tensile strain rate of $10^{-3} s^{-1}$. High-resolution optical technique, which involves optical acquisition with a CCD camera, was used to determine the shear strain $\gamma = 2\varepsilon_{12}$ in the central part of the specimen. Monotonic and Bauschinger simple shear tests for different amount of forward shear prestrain 10%, 20% and 30% are performed in order to examine the stress-strain anisotropy, the Bauschinger effect. It is worth noting that the simple shear loading induces large texture rotation and yields to different anisotropic behavior compared to the classical uniaxial tensile test.

2.2.3. Equi-biaxial tensile test

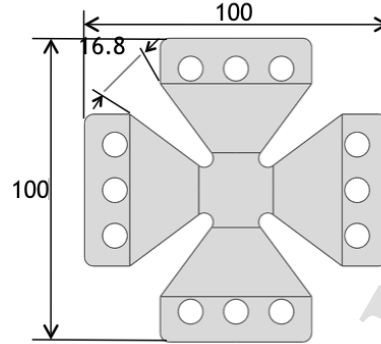


Figure 2: equi-biaxial tensile specimen geometry and dimensions.

In order to characterize the plastic anisotropy of the material, equi-biaxial tests were carried out on the specimen shown in figure 2, obtained using a hyperbar waterjet. The displacement rate is 0.02mm/s along both rolling direction (RD, direction 1) and transverse direction (TD, direction 2) at the same time till the rupture. Since the gauge area is a $20 \times 20\text{mm}^2$ square, the strain rate is around 10^{-3}s^{-1} .

2.2.4. Meuwissen tensile test

This mechanical test is a non standard tensile test proposed by [36, 37] in order to have heterogeneous strain fields. In the present study, the Meuwissen sample geometry is however modified in order to optimize the strain gradient temporal distribution and higher heterogeneous stress/strain fields, as shown in figure 3. The sample geometry is complex, and is obtained using a hyperbar waterjet. The load is applied using a standard uniaxial tensile-testing machine.

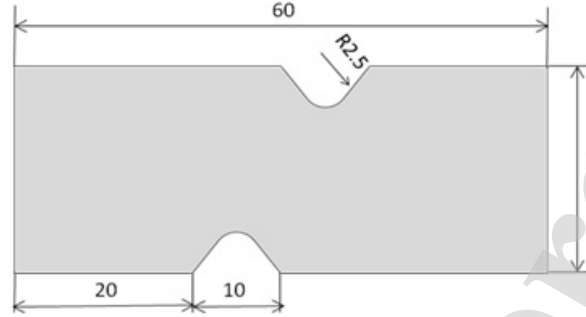


Figure 3: Specimen used for Meuwissen tensile test

The specimen is loaded under displacement control by moving the upper clamp upwards whereas the lower clamp is fixed. Two loading directions are adopted: rolling and transverse directions (respectively 0° and 90° with respect to the rolling direction). The experiments are carried out at room temperature and the crosshead velocity is 0.066 mm/s corresponding to an average strain rate of $1.710 \cdot 10^{-3} \text{ s}^{-1}$.

3. Experimental results

3.1. Uniaxial tensile test

True stress versus true strain curves are depicted in Figure 4(a). The material displays strong in-plane anisotropy. The loading along rolling direction corresponds to the lowest stresses for all the plastic strain, whereas transverse direction, displays the highest stress level. The relative variation in stress between the lowest and the highest values is about 37.7% at a true strain of 15% and demonstrates the large degree of planar anisotropy in this material. The amount of total uniform elongation reaches the highest level (more than 35%) for loading along the rolling axes and decreases when the loading direction moves away from this direction (less than 20% for transverse direction). Overall, the uniform elongation under monotonic loading remains relatively high. The work-hardening evolution is also sensitive to the direction of loading. The initial yield

stresses estimated for an offset of 0.1% plastic strain clearly denote considerable initial in-plane stress anisotropy (see Figure 4(b)).

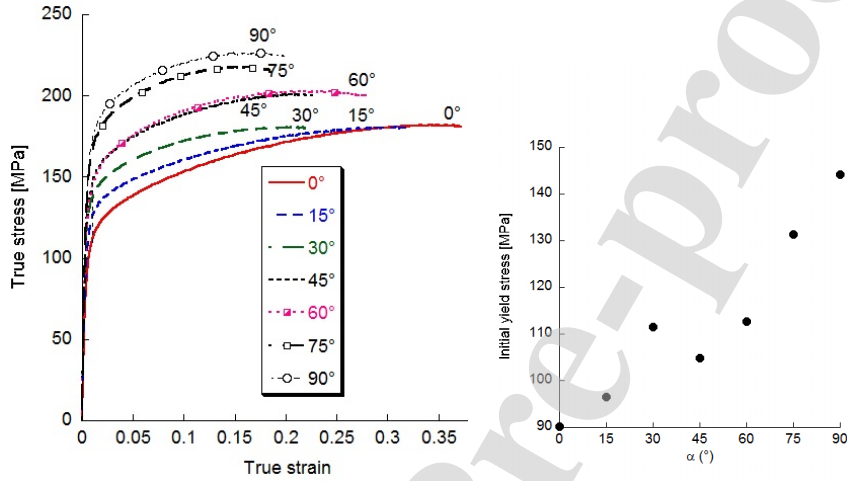


Figure 4: (a) True stress vs true strain for different monotonic uniaxial tensile tests along different directions with respect to the rolling direction (b) Initial yield stresses

The work-hardening evolution θ normalized by the elastic shear modulus μ ($\approx 30\text{GPa}$) is given as a function of the increase in yield stress i.e. $\sigma - \sigma_0$ in Figure 5(a). For low values of plastic strain (and thus $\sigma - \sigma_0$), the work-hardening is very high $\theta/\mu > 1/5$, and significant variation of θ/μ with respect to the loading direction is observed. However, as $(\sigma - \sigma_0)$ increases, the material appears to experience similar work-hardening irrespective of orientation and θ/μ decreases rapidly below $1/30$ to reach a steady state value of $\sim \mu/150$.

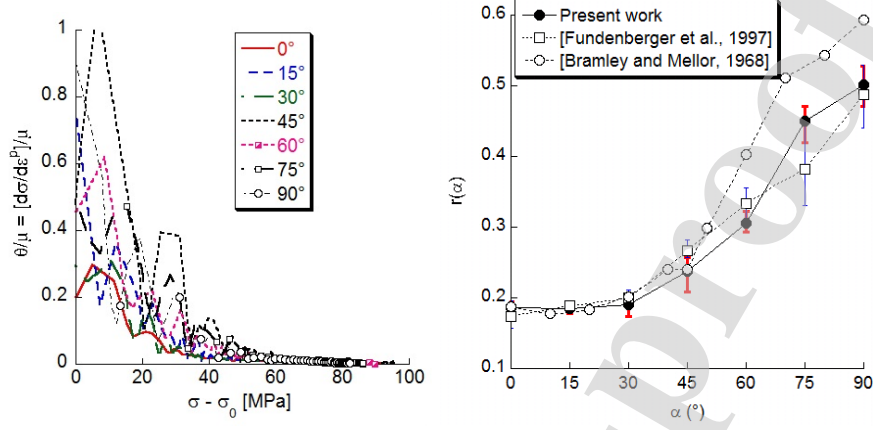


Figure 5: (a) Work-hardening vs amount of stress increase for different monotonic uniaxial tensile tests along different directions with respect to the rolling direction (b) Variation of r-value with orientation and comparison with data from literature on similar material

Anisotropy is determined by calculating the r-values (Figure 5(b)) and their evolution with plastic strain (an example is given in Figure 6(a) for tension along 0°, 45° and 90° orientations).

All the plotted data correspond to an average over three measured for each orientation. For comparison purpose, data previously obtained by [12, 27] on similar material, are indicated on Figure 5(b). Substantial variation in r-value is observed, denoting the high in-plane strain anisotropy of the material. The degree of planar anisotropy in the zinc is very different from that existing in other HCP materials (e.g. pure titanium [38], magnesium based materials). The r-values are very low and below unity. It is worth noting that r-values greater than unity indicate higher material resistance to thinning when subjected to biaxial tensile stresses in the sheet plane and therefore better drawability. Such behavior is favorable to good performance for forming processes when different parts of the blank are subjected to stretch-forming and radial drawing. As the studied Zn-Cu-Ti rolled sheet displays r-values lower than unity, this material has low resistance to thinning, at least under monotonic loading. The high uniform elongations observed under uniaxial tensile test indicate that the de-

formation is mainly compensated by significant thickness reduction along the whole gauge area.

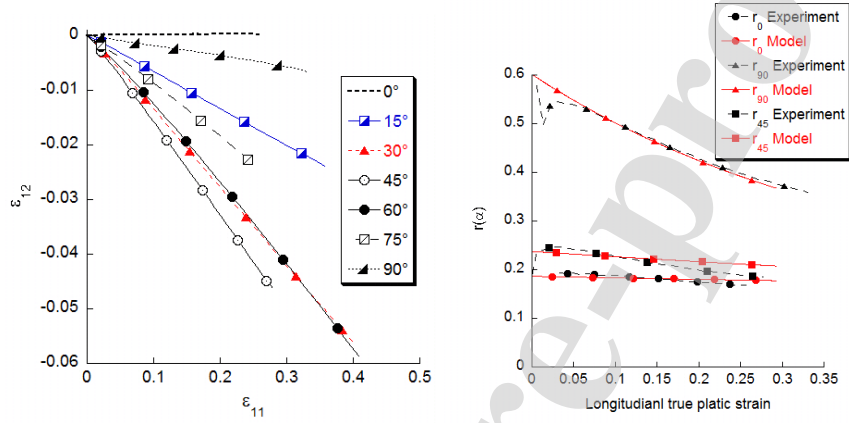


Figure 6: (a) Shear strain evolution for uniaxial tensile test along different orientations with respect to the rolling direction, (b) R-value evolutions with longitudinal true plastic strain along 0°, 45° and 90°, model corresponds to equation (1)

Finally the material anisotropy is examined by analyzing the evolution of shear component for the different loading directions. Figure 6(a) indicates the distribution of the shear component ε_{12} versus the longitudinal strain ε_{11} for the different tensile tests. We note that the shear strain component ε_{12} is almost zero when loaded along the rolling (RD) as well as the transverse directions (90°/RD). However, ε_{12} increases by 0.1 for every 2° rotation of the loading axis about the RD, reaching a maximum value when the loading axis is along 45°/RD. It bears mentioning that this behavior cannot be properly explained using the classical yield models [5], including those adapted to Hexagonal materials [39], the reason being that the yield parameters themselves vary with increasing plastic strain (as seen in figure 6(b)), i.e. as the test progresses.

In order to describe the measured r-values as seen in figure 6(b), noting the shape of the curve, we introduce the following evolution law:

$$r_{\alpha}(\bar{\varepsilon}^p) = r^{exp,i} + a_{\alpha}(e^{-c_{\alpha}\bar{\varepsilon}^p} - 1) \quad (1)$$

where $r^{exp,i}$ is the initial experimental r-value for tensile test along α , $\bar{\varepsilon}^p$ is the equivalent plastic strain, a_{α} and C_{α} are 2 material parameters that need to be identified (see Table 2).

Parameter	0°	45°	90°
a_{α}	0.186	0.22	0.45
C_{α}	1/6	0.5	2.5

Table 2: Material parameters for the description of the evolution of $r(\alpha)$.

The law in (1) has also been plotted in Figure 6(b), for $\alpha = 0^{\circ}$, 45° and 90° .

3.2. Simple shear test

Forward and reverse shear tests give information about loading-related anisotropy and kinematic hardening in the material. From a micro-structural point of view, this could be due to de-twinning or dislocation pile-ups during the unloading stage.

The reverse simple shear tests were carried out on specimens cut out from the as-received material at various angles to the rolling direction, namely 0° , 45° and 90° . These tests were conducted up to a forward amount of shear strain of about 10%, 20% and 30% followed by reversed shear up to -40% (which corresponds respectively to $\approx 34.6\%$, 46% and 57.7% von Mises equivalent accumulated true strain, which is higher than the uniform elongation observed in uniaxial tension). The stress-strain curves are used in order to analyze (i) the work-hardening evolution at large strain, (ii) the Bauschinger effect and its evolution as function of amount of forward prestrain, (iii) the occurrence of transitory regime under stress reversal.

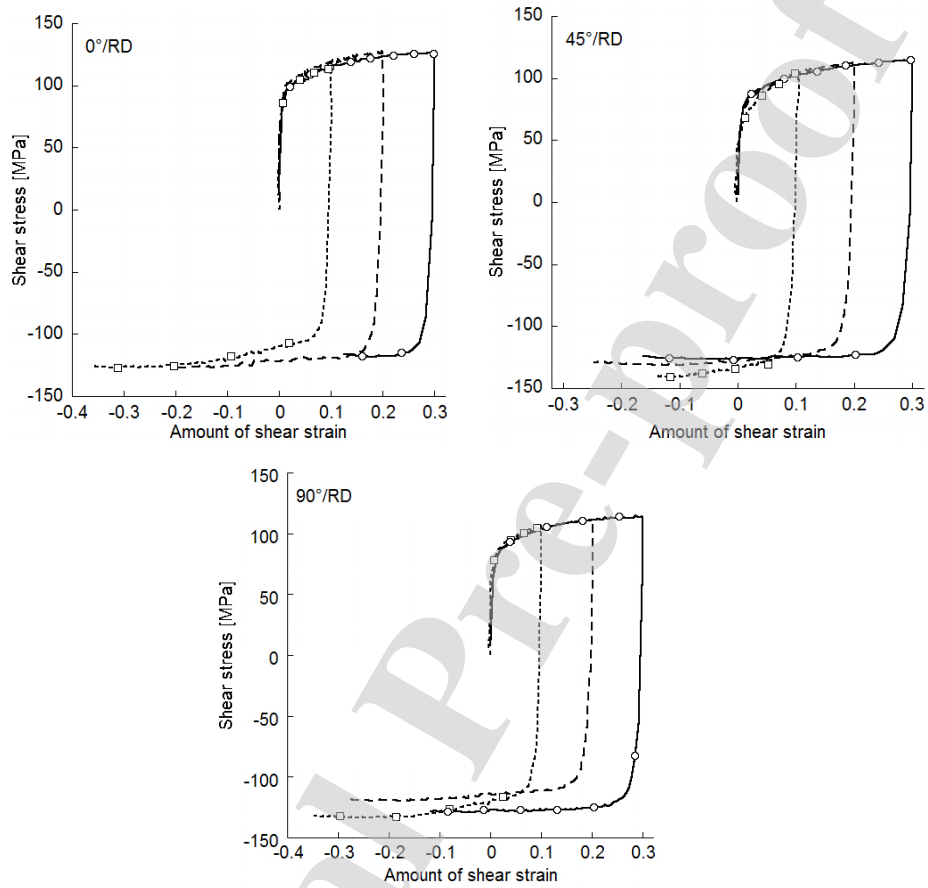


Figure 7: Stress-strain curves for reverse simple shear loading along three directions with respect to the rolling direction (0° , 45° and 90°). The tests are performed for three levels of forward amount of shear strain 10%, 20% and 30%.

Overall, the results obtained, by repeating each test 3 times, are fairly consistent. The stress-strain curves are shown in Figure 7 where the vertical axis indicates the shear stress and the horizontal axis refers to amount of shear strain.

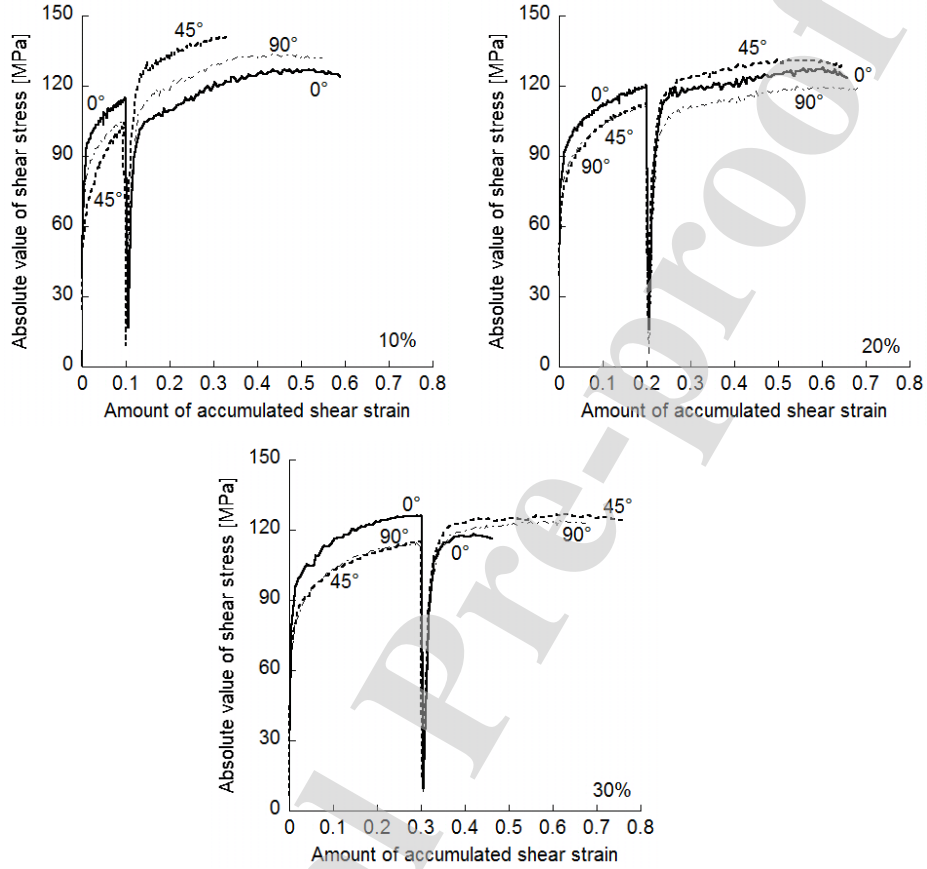


Figure 8: Absolute shear stress versus accumulated absolute amount of shear strain curve for simple shear loading.

To examine the anisotropic behavior under simple shear loading, the stress-strain curves are plotted using an accumulated amount of shear strain and plotted for similar amount of forward shear strain (Figure 8). Similar to the uniaxial tensile test, the material displays significant stress anisotropy. Note that upon strain reversal, the loading along 45°/RD displays the highest stress level. When the amount of forward shear strain is low (i.e. 10% in the present case), material work hardening is observed along the reverse loading (i.e. the shear stress increases after strain reversal). However, some stress saturation is clearly observed for 30% amount of forward shear strain.

Given that at 10% strain, the material ductility is highest along 0° /RD and lowest along 45° /RD under shear loading we would expect the opposite under uniaxial tensile loading. However, as shown in figure 4, this is not the case, indicating that the activation of physical mechanisms is load dependent *ergo* the ductility is *highly* dependent on loading condition (in terms of loading direction and level of forward shear strain).

There is some anisotropy before the load reversal as can be seen from the figure 8. The material is stiffer along 0° /RD compared to along 45° /RD and 90° /RD which seems to contradict the result obtained during uniaxial tensile tests but in fact demonstrates the equivalence of tensile loading along 0 and shear loading along 45° /RD.

The extreme variation of behavior between 0 and 90° /RD *after* load reversal is due to anisotropic physical mechanisms, in particular, the activation of the twinning mode (which is not reversible) after unloading and reloading [25].

It bears mentioning that Butcher, Abedini and others [40, 41, 42] have suggested the Logan-Hosford model for the shear to equivalent stress ratio to describe the yield in anisotropic materials where the plastic deformation involves twinning (such as Magnesium). Inverse analysis using the above model to fit our experimental data is a potential area of future work.

Furthermore, the Bauschinger effect is relatively high, thus implying significant kinematic hardening.

3.3. *equi-biaxial tensile test*

Figure 9 shows the force-displacement curves for equi-biaxial tensile tests. As in uniaxial tensile test, the material response shows a highly anisotropic behavior and the rolling direction corresponds to the softer direction.

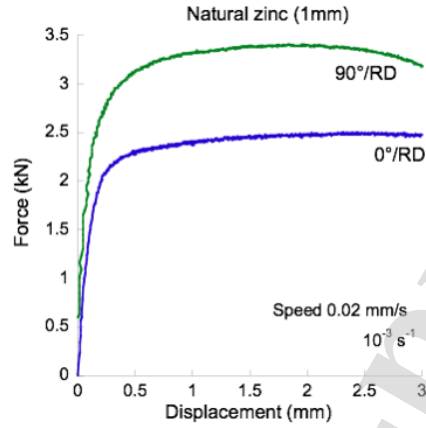


Figure 9: Force versus displacement curves of equi-biaxial tensile tests.

Figures 10(a) and 10(b) show the full field strain distribution for two different displacement increments corresponding to (a) $t = 10s$ just before the beginning of the heterogeneous strain field distribution and (b) $t = 50s$. In Figure 10(a), the strain distributions are almost homogeneous ($< 0.5\%$) in longitudinal, transverse as well as shear. Even though it seems that shear strain is more concentrated in the corners of the sample, the strain level is quite low (around 0.2%). However, as seen in the figure 10(b), the homogeneous area decreases a lot with only a small square in the centre of gauge area retaining a low homogeneous strain level, which is 2% in longitudinal, 2.4% in transverse and 0.3% in shear. Meanwhile, it is easy to observe that the longitudinal, transverse and shear strains reaches high values of : 4.5% , 5.9% and 3% respectively in the corners of the gauge area.

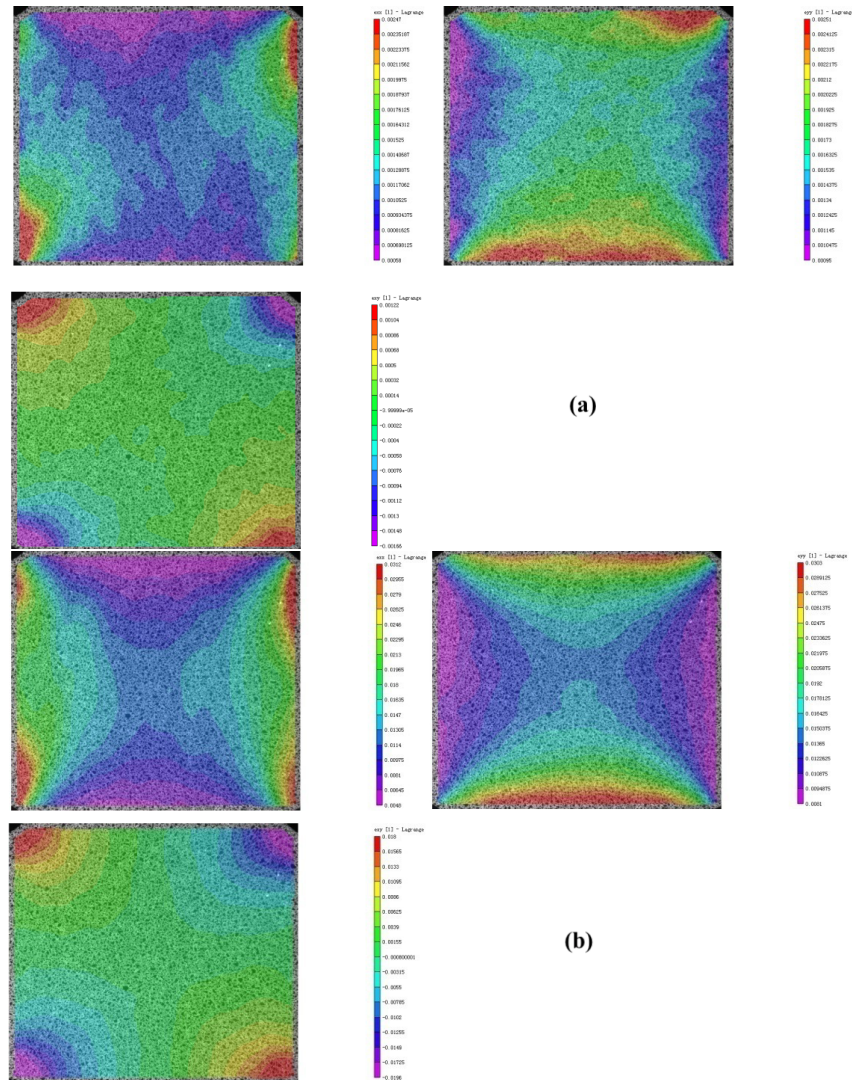


Figure 10: Full field strain distribution for the equibiaxial test (top left: longitudinal strain, top right: transverse strain and bottom left: shear strain) (a) at $t = 10s$ (end of the homogeneous strain distribution) and (b) at $t = 50s$

Figure 11 shows the true stress versus true strain curves in the gauge area. The work hardening evolution is different from what was observed in the simple shear and uniaxial tensile loading tests. Similar work-hardening evolution is

observed along both directions (RD and TD).

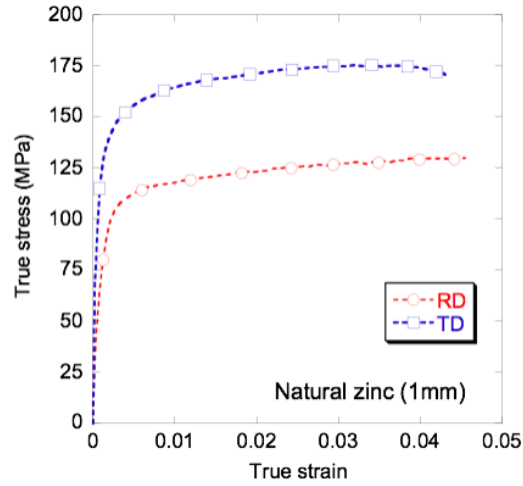


Figure 11: True stress vs. true strain in gauge area during equi-biaxial tensile test.

3.4. Heterogeneous strain fields using Mewissen geometry

The force-displacement curves are given in Figure 12 for both loading directions (i.e. tension along RD or TD direction). The corresponding strain fields are given in Figures 13(a), 13(b) and 13(c) before rupture. As for the homogeneous tests, the material response is highly anisotropic.

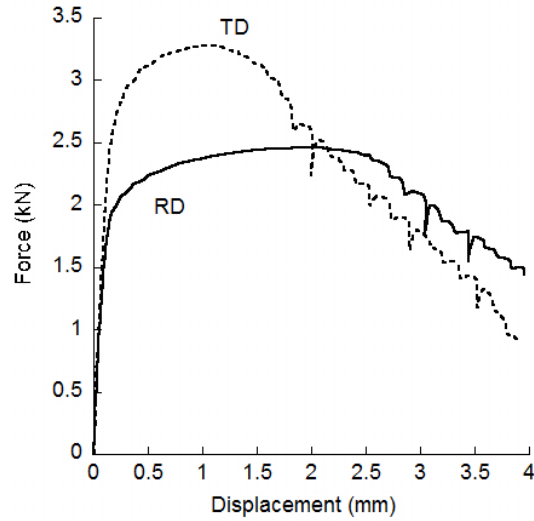


Figure 12: Force-displacement curves for Meuwissen test, tension along RD or TD.

The maximum longitudinal strain (Figure 13) is about 0.4 to 0.5 true strain when the loading is along the rolling direction and decreases to 0.2 when the loading is along the transverse direction.

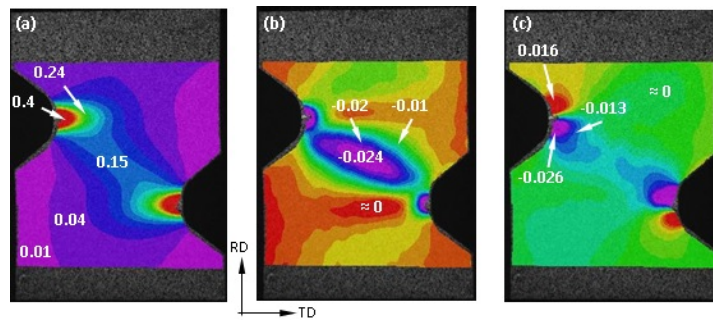


Figure 13: Meuwissen geometry, tension along RD. Experimental (a) longitudinal, (b) transverse and (c) shear strain distribution. RD: Rolling direction, TD: Transverse direction.

4. Constitutive mechanical model

The material flow characteristic is governed by the initial anisotropy in addition to other material properties. Phenomenological plasticity theories consider initial anisotropy through a yield criterion and strain hardening laws.

4.1. Yield surface

In the present work, in addition to the isotropic von Mises yield criterion, two anisotropic yield surfaces description have been considered: the classical [5] and a non quadratic [39] criterion developed for a better description of significantly anisotropic materials. For [5], its general form is given by:

$$\boldsymbol{\Sigma} : \mathbf{H} : \boldsymbol{\Sigma} = (\boldsymbol{\sigma}' - \mathbf{X}) : \mathbf{H} : (\boldsymbol{\sigma}' - \mathbf{X}) = \sigma_Y^2 \quad (2)$$

where $\boldsymbol{\Sigma} = \boldsymbol{\sigma}' - \mathbf{X}$ is the effective deviator stress tensor, σ_Y is the flow stress, \mathbf{H} is a purely deviatoric tensor corresponding to the quadratic Hill criterion described by 6 components F, G, H, L, M and N , \mathbf{X} is the back stress tensor (kinematic hardening) and $\boldsymbol{\sigma}'$ is the deviatoric part of the Cauchy stress tensor $\boldsymbol{\sigma}$. When no kinematic hardening is present, this simplifies to:

$$F(\sigma_y - \sigma_z)^2 + G(\sigma_z - \sigma_x)^2 + H(\sigma_x - \sigma_y)^2 + 2L\sigma_{yz}^2 + 2M\sigma_{zx}^2 + 2N\sigma_{xy}^2 = \sigma_Y^2 \quad (3)$$

where x, y and z are the axis of orthotropy (e.g. in case of sheet material, the rolling, the transverse and the normal directions). σ_i is the normal stress component according to the i axis and σ_{ij} is the shear stress component of the stress tensor $\boldsymbol{\sigma}$.

The success of this criterion is associated to its numerical simplicity, identification easiness and its availability in several commercial FE codes. It is worth noting that in case of sheet materials, through thickness mechanical characterization of the material anisotropy is a hard task. Therefore, in the criteria investigated in this work, the related material parameters (L and M in this case) are fixed at their values in case of isotropic behavior. To describe yielding of orthotropic materials, [39] developed an original approach based on the generalization to orthotropy of the J_2 and J_3 invariants of the deviatoric stress tensor

σ' . Such generalized invariants are used in the [43] isotropic criterion in order to introduce the anisotropy:

$$(J_2^0)^3 - c(J_3^0)^2 = 27(\sigma_Y/3)^6 \quad (4)$$

where

$$J_2^0(\boldsymbol{\sigma}) = \frac{a_1}{6}(\sigma_x - \sigma_y)^2 + \frac{a_2}{6}(\sigma_y - \sigma_z)^2 + \frac{a_3}{6}(\sigma_x - \sigma_z)^2 + a_4\sigma_{xy}^2 + a_5\sigma_{xz}^2 + a_6\sigma_{yz}^2 \quad (5)$$

and

$$\begin{aligned} J_3^0(\boldsymbol{\sigma}) = & \frac{1}{27}(b_1 + b_2)\sigma_x^3 + \frac{1}{27}(b_3 + b_4)\sigma_y^3 + \frac{1}{27}(2b_1 + 2b_4 - b_2 - b_3)\sigma_z^3 \\ & - \frac{1}{9}(b_1\sigma_y + b_2\sigma_z)\sigma_x^2 - \frac{1}{9}(b_3\sigma_z + b_4\sigma_x)\sigma_y^2 - \frac{1}{9}[(b_1 - b_2 + b_4)\sigma_x \\ & + (b_1 - b_3 + b_4)\sigma_y]\sigma_z^2 + \frac{2}{9}(b_1 + b_4)\sigma_x\sigma_y\sigma_z \\ & - \frac{\sigma_{xz}^2}{3}[2b_9\sigma_y - b_8\sigma_z - (2b_9 - b_8)\sigma_x] - \frac{\sigma_{xy}^2}{3}[2b_{10}\sigma_z - b_5\sigma_y - (2b_{10} - b_5)\sigma_x] \\ & - \frac{\sigma_{yz}^2}{3}[(b_6 + b_7)\sigma_x - b_6\sigma_y - b_7\sigma_z] + 2b_{11}\sigma_{xy}\sigma_{xz}\sigma_{yz} \quad (6) \end{aligned}$$

x, y and z are the directions of the orthotropic frame. This criterion involves 18 material parameters $c, b_1 \dots b_{11}, a_1 \dots a_6$ for general 3D anisotropy (with $b_1 \dots b_{11}$ and $a_1 \dots a_6$ reducing to unity under isotropic conditions). For sheet metal anisotropy where only the in-plane stresses are non-zero, the 18 parameters reduce to 11 : $c, b_1 \dots b_5, b_{10}, a_1 \dots a_4$, with the rest of the parameters retaining their isotropic values (i.e. = 1).

4.2. Strain hardening

The hardening is described using Voce isotropic hardening as given below:

$$\sigma_Y(\bar{\epsilon}_{pl}) = Y_0 + R_{sat}(1 - e^{-c_R \bar{\epsilon}_{pl}}) \quad (7)$$

where Y_0 is the initial yield stress, C_R and R_{sat} are the rate and the saturation value of the isotropic hardening, respectively.

5. Inverse parameter identification, part I : Yield parameters from experiments

The first step of material parameters identification concerns the description of the initial material anisotropy. For the Hill criterion [5], the parameters are determined following the classical methodology using only the experimental r-values r_0 , r_{45} and r_{90} and σ_0^0 for the initial yielding using the relation $\sigma_Y = f(\sigma_{11}, \alpha)$, where 1 is the tensile direction, σ_{11} is the tensile true stress and α is the angle between the tensile direction and the orthotropic axes x . The results are shown in Table 3.

The identification of the Cazacu and Barlat (CB2001) [39] anisotropy parameters (Table 4) is complex and a special in-house code (DD3MAT) developed for this purpose was used to guarantee the best fit to the experimental data [44].

The identification of the constitutive parameters involved: (i) uniaxial tensile tests with samples taken at intervals of 15° orientation with respect to the rolling direction and (ii) monotonic simple shear tests with samples taken at 0° , 45° and 90° orientations with respect to the rolling direction. This means that 17 experimental results were used to identify the parameters (seven r-values, seven uniaxial and three simple shear initial yield stresses).

For comparison purpose, the material parameters for the Hill criterion [5] are

	F	G	H	N
using only $r_0, r_{45}, r_{90}, \sigma_0^0$	0.31	0.84	0.157	0.85
using all $\sigma_0^0, \sigma_0^{15}, \dots, \sigma_0^{75}, \sigma_0^{90}$ and $r_0, r_{15}, r_{30}, \dots, r_{75}, r_{90}$	0.46	1.26	0.23	1.26

Table 3: Material parameters for Hill criterion [5]

c	a_1	a_2	a_3	a_4	b_1	b_2	b_3	b_4	b_5	b_{10}
-0.906	1.27	-0.02	0.8	0.99	-0.6	8.7	3.9	-2.1	0.4	0.91

Table 4: Material parameters for Cazacu and Barlat criterion [39]

also identified using all the experimental data listed above. The identified material parameters are given in Table 3 for Hill [5] and Table 4 for [39].

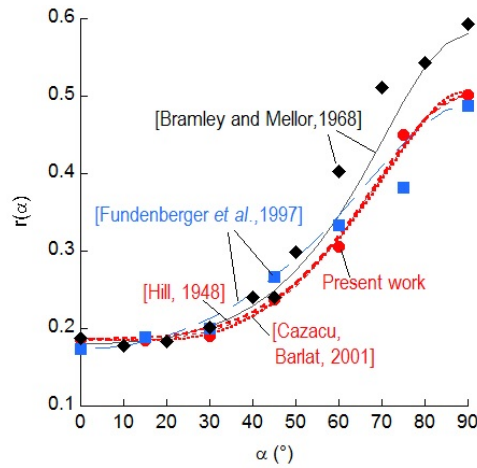


Figure 14: r-value prediction using $(\sigma_0^0, r_0, r_{45}, r_{90})$ for the identification of F, G, H and N or the set of all experimental data (present work). The results obtained using the Cazacu-Barlat criterion [39] are also indicated. For comparison purpose, data from Bramley and Mellor [12] and Fundenberger et al [27] are provided.

Figure 14 and Figure 15 indicate that the r-value as well as the initial yield stresses evolutions are relatively well described by both [5] and [39], however, the corresponding yield surfaces are radically different (Figure 16), which highlights the difference in modeling the anisotropic behavior using these two yield criteria. Significant differences are observed along biaxial loading which seems to be required for a better assessment of the efficiency of the adopted models in describing the behavior of zinc sheet material.

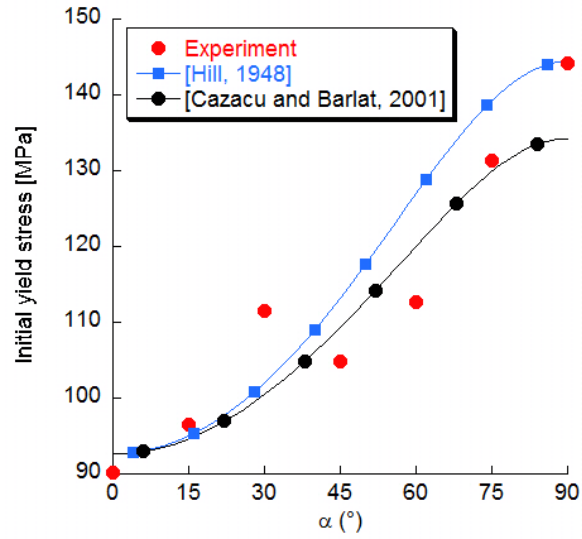


Figure 15: Initial yield stresses described using the Hill [5] and the Cazacu-Barlat [39] criteria

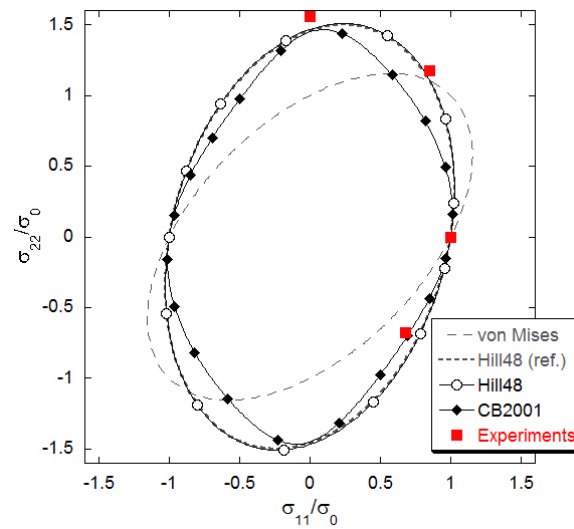


Figure 16: Yield surface description. Hill48(ref) corresponds to the model using material data parameters identified with $(\sigma_0^0, r_0, r_{45}, r_{90})$. Hill48 refers to the model using material data parameters identified with all experimental data. CB2001 is the yield surface obtained using Cazacu and Barlat's criterion [39].

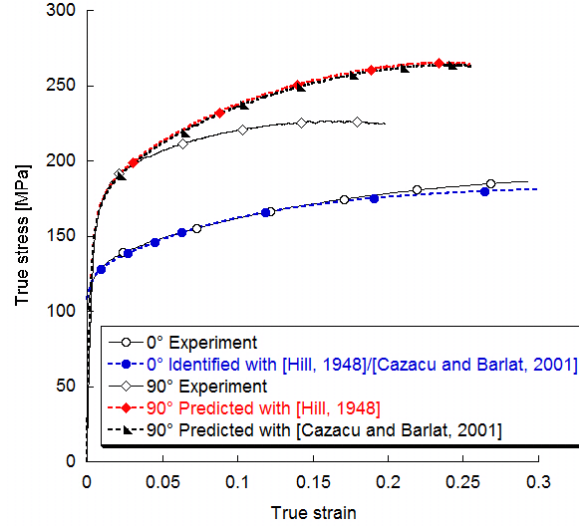


Figure 17: Predicted strain-stress response for uniaxial tensile test along transverse direction using material parameters identified on uniaxial tensile test along rolling direction.

Figure 15, while showing good agreement with the experiments, shows only the *initial* yield stresses. The agreement between the experimental and predicted curves needs to be examined in terms of stress and work-hardening *evolution*. An example is provided in figure 17 for the prediction of the stress-strain response during the uniaxial tensile test along TD using data identified on uniaxial tensile test along RD. Note that these predicted curves were obtained assuming that the material parameters in the description of the yield surface remain constant.

One can notice that the Hill criterion [5] fails to correctly describe the highly anisotropic material behavior along 90° . In fact, for the investigated material, even more advanced yield criteria [39] (specially adapted to hexagonal materials) appear to fail to describe the observed behavior along 90° . As previously shown in Figure 6, the measured evolution of the r -values indicates that their sensitivity to the plastic strain can be very high, particularly along 90° . This sensitivity needs to be taken into account during the identification of the material parameters for Hill criterion [5] as proposed by Nixon et al [45].

6. Inverse parameter identification, part II : hardening parameters using Finite Element simulation

Finite element simulations have been performed in order to model the mechanical tests carried out on the material under investigation (uniaxial tension, equi-biaxial tension and Meuwissen tension). In all these simulations, the parameters of the yield criterion are kept constant (Hill [5]) as calculated from the Lankford coefficients in section 5. However, the Voce hardening parameters R_{sat} , C_R as well as the initial yield stress Y_0 adopted in the isotropic hardening law (equation 7) are identified by a second inverse analysis to get the best fit for the tensile test's force-displacement or stress-strain material response. The hardening parameters are the same for all three tests (uniaxial, equi-biaxial and Meuwissen test).

6.1. Uniaxial tension

Figure 18 shows the geometry of the specimen (as used in the experimental test), the FE-mesh, loading conditions and displacement constraints.

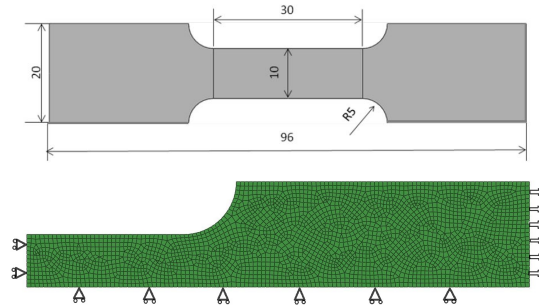


Figure 18: Geometry of the specimen (top), FE-mesh of the upper right quarter of the specimen, and boundary condition in modeling the uniaxial tension, length unit is mm.

Assuming symmetrical loading conditions, the FE-simulation is performed on a quarter of the piece, with thickness 1 mm, under uniaxial tension along $0^\circ/\text{RD}$, $45^\circ/\text{RD}$ and $90^\circ/\text{RD}$. The displacement of the bottom and right boundaries are imposed, the vertical displacement of bottom is fixed while the right

boundary is moved to a maximum displacement of 4 mm at a rate of 0.2 mm/s. Horizontal displacement of the surface on the left is blocked. The model has been discretized by 2831 4-noded bilinear plane stress elements with reduced integration of type CPS4R (implemented in ABAQUS). Triangular elements, different orders of integration as well as mesh sizes have been tested to ensure the convergence of the FE-mesh, i.e. the results are mesh-independent.

The mechanical behavior of the material is composed of two distinct portions: a linear isotropic elastic part and a plastic hardening part. The elastic portion of the material behavior is described by Hooke's law ($E = 81\text{GPa}$, $\nu=0.33$). As for the plastic behavior, isotropic Voce hardening has been assumed since this law is often used for describing plastic deformation for alloys which exhibit a saturation stress-strain state at high strain levels which is observed for the current Zinc alloy. The three Voce hardening parameters in equation (7) need to be identified using optimization and inverse analysis.

Let $\mathbf{x}^* \in \mathcal{R}^3$ represent the vector of three material parameters to be identified, then the optimization problem may be posed as:

$$\begin{aligned} & \text{Find : } \mathbf{x}^* = \underset{\mathbf{x} \in \mathcal{R}^3}{\text{Arg min}} \mathcal{J}(\mathbf{x}) \\ & = \underset{\mathbf{x} \in \mathcal{R}^3}{\text{Arg min}} \frac{|\epsilon_{0^\circ}(\mathbf{x})| + |\epsilon_{45^\circ}(\mathbf{x})| + |\epsilon_{90^\circ}(\mathbf{x})|}{3} \end{aligned} \quad (8)$$

where the objective function $\mathcal{J}(\mathbf{x})$ is the mean of the absolute values of the errors $\epsilon_{0^\circ}(\mathbf{x})$, $\epsilon_{45^\circ}(\mathbf{x})$ and $\epsilon_{90^\circ}(\mathbf{x})$ between the simulated and experimental tensile curves along $0^\circ/\text{RD}$, $45^\circ/\text{RD}$ and $90^\circ/\text{RD}$ respectively.

The optimization strategy we have adopted is a combination of the Genetic Algorithm and the Simplex algorithm implemented in MATLAB. In the first phase, we use a Genetic Algorithm to maximize our chances of obtaining a global converged result. The GA result is then selected as a starting point for the second phase, a Simplex search to find the closest local minimal function value. The GA parameters are set as follows: starting point (185.90 199 1370.1); population size 50; crossover fraction 0.8; mutation 0.01. After 66 generations the GA is stopped since the objective function tolerance is less than $1e-6$ while

the objective function value from equation (8) is 21.55.

The settings for the Simplex are: starting point (101.11 180.24 1585.27), x tolerance $1e-6$; objective function \mathcal{J} tolerance $1e-6$. After 116 generations the optimal solution is seen to converge with an objective function value of 19.83. The iteration history for both phases of the identification is given in Figure 19.

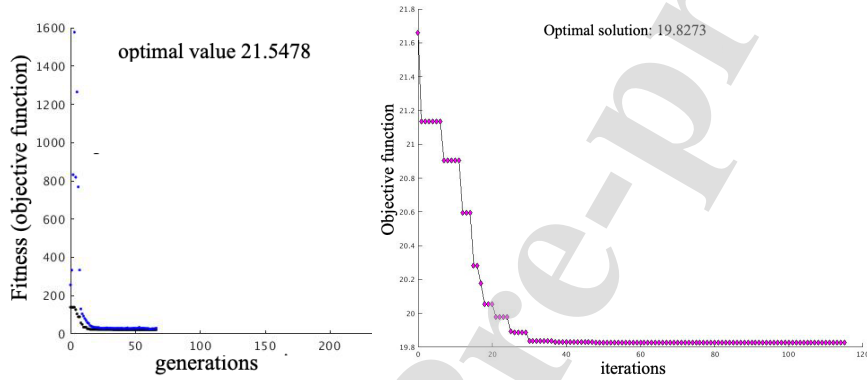


Figure 19: Iteration history of the GA (first phase) and Simplex (second phase) procedures

Hill coefficient	F	G	H	N	L	M
Value	0.31	0.84	0.157	0.85	1.5	1.5
Voce parameter	Y_0		R_{sat}		C_R	
Value	100.93 MPa		174.19 MPa		2107.94	

Table 5: Identified Hill yield and Voce hardening parameters (using uniaxial tensile testing).

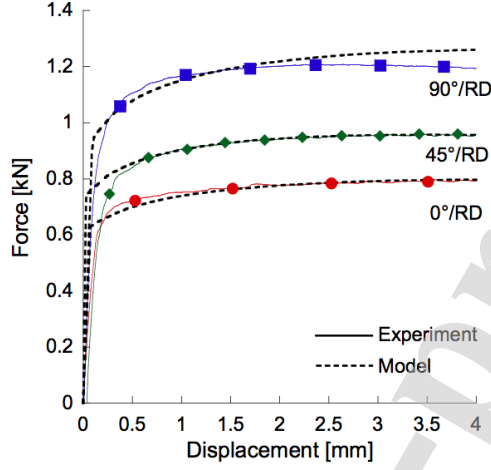


Figure 20: Comparison of force-displacement curves obtained by FE simulation and experimental tests for uniaxial tension along $0^\circ/\text{RD}$, $45^\circ/\text{RD}$ and $90^\circ/\text{RD}$.

The optimal solution to the inverse problem, i.e. the best choice for the three hardening parameters for the chosen hardening law, that can *simultaneously* approximate the uniaxial force-displacement responses along $0^\circ/\text{RD}$, $45^\circ/\text{RD}$ as well as $90^\circ/\text{RD}$, is given in Table 5. The associated force-displacement curves are shown in Figure 20. There is a reasonably good agreement between the simulated and the experimental curves with the optimal solution $J(\mathbf{x}^*) = 19.83$.

6.2. Equi-biaxial test

The main interest of the equi-biaxial test lies in the strain field observed in the middle of a specimen from an isotropic homogenous material, similar to the uniaxial tensile test. The finite element mesh and loading conditions are described in Figure 21. The four arms of the specimen are subjected to a maximum displacement of 4 mm at a displacement rate of 0.2 mm/s. The model has been discretized by 12201 4 noded bilinear plane stress elements with reduced integration (type CPS4R in ABAQUS). The mesh is refined in the central region since the deformation is primarily in this region, based on our

experimental results. We have tested different sizes of mesh to ensure mesh-independency of our results.

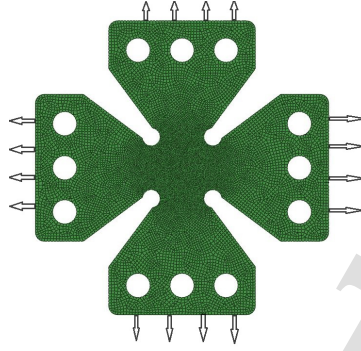


Figure 21: FE-mesh and boundary conditions (right).

Just as in the case of the uniaxial tensile test, the isotropic linear elastic domain of the studied material is described using the Hooke's law with the same values for the Young's modulus and Poisson's ratio, while its anisotropic non-linear behavior is given by the Hill criterion [5] with Voce isotropic hardening (parameters Y_0 , R_{sat} and C_R). The material parameters used are those that have been obtained in the previous subsection using inverse identification and tensile testing along the three directions, and are given in Table 5.

We observe in figure 22 that the simulated force-displacements are in good agreement with the experimental data for both $0^\circ/\text{RD}$ and $90^\circ/\text{RD}$. It can be observed that the yield point is well predicted along $90^\circ/\text{RD}$ while the plastic simulated response is higher than that experimentally observed, this phenomenon could be attributed to the onset of damage in the experimental specimen.

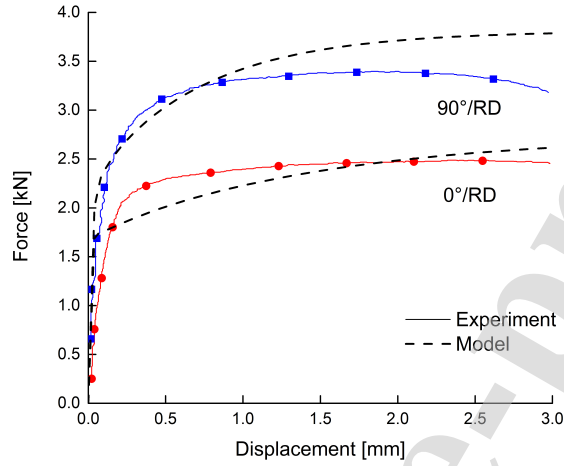


Figure 22: Force and displacement curves by FE simulations and experiments

As can be seen in Figure 23, the FE results are almost similar to the experimental ones. The strain distributions (longitudinal, transverse and shear strain) have a similar trend as the experimental values, though they may not have the same exact values. At this stage, the identification procedure performed assuming a phenomenological constitutive law seems to be well adapted for estimating the behavior of the Zinc based alloy studied here.

6.3. Meuwissen test

In order to test the validity of the chosen constitutive laws and associated parameters, the Meuwissen test is considered, since it creates heterogeneous strain fields in the specimen as mentioned in section 2.2.4. This test is especially adapted in this work due to the anisotropy of Zinc based materials. The finite element mesh, loading and boundary conditions are described in Figure 24. The displacements of the left and right edges of the specimen are imposed : on the left, the longitudinal displacement is blocked while, on the right, a longitudinal displacement of 4mm is imposed at a rate of 0.2 mm/s. The physical domain has been discretized by 8281 4-noded bilinear plane stress elements with

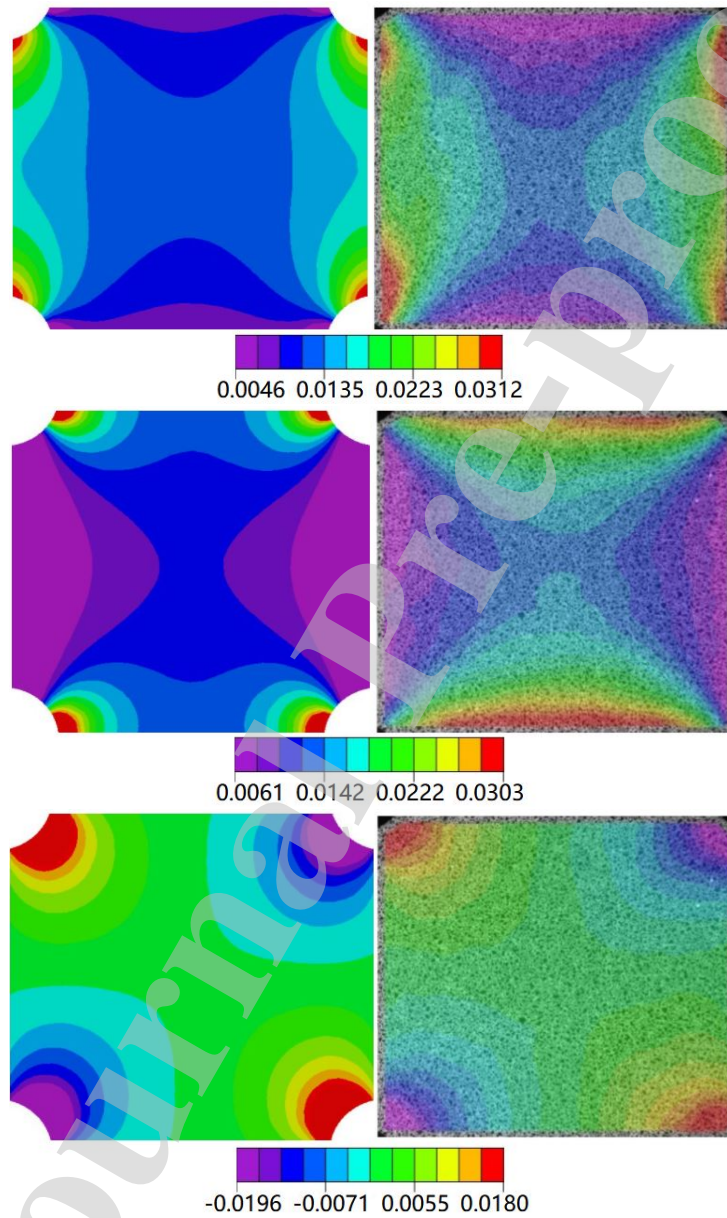


Figure 23: Strain fields for ε_{11} , ε_{22} and ε_{12} obtained by FE simulation and experiments at $t=50$ seconds.

reduced integration (type CPS4R in ABAQUS), the mesh is refined in the vicinity of the "notches", since the deformation is primarily located in this region based on our experimental results. Different mesh sizes have been considered to ensure mesh independence of our results.

The mechanical behavior is the same as that assumed in the two previous tests,

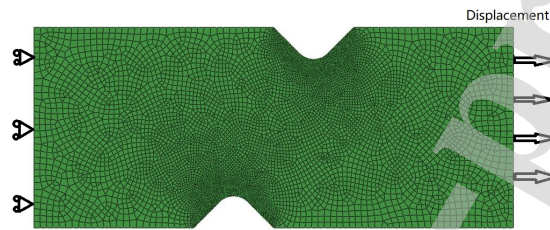


Figure 24: FE-mesh of the specimen, and boundary conditions used for modeling the Meuwissen test.

with the associated material parameters having been obtained in the identification procedure on the different tensile tests and given in Table 5.

Figure 25 shows that by using these parameters, the experimental results in term of force-displacement are well predicted by the simulation until the onset of necking.

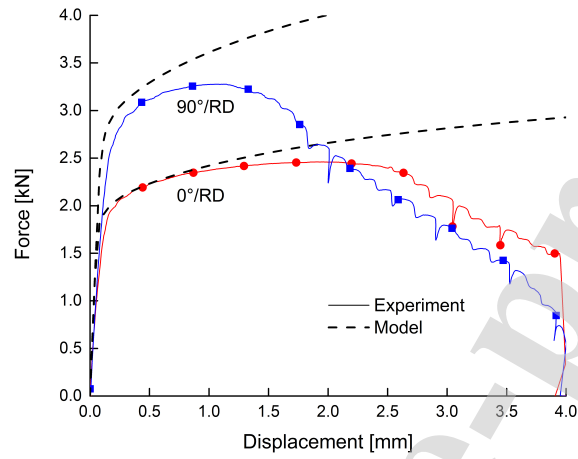


Figure 25: Comparison of Force-Displacement curves from the FE simulation and the experimental tests, for Meuwissen tension along RD and TD.

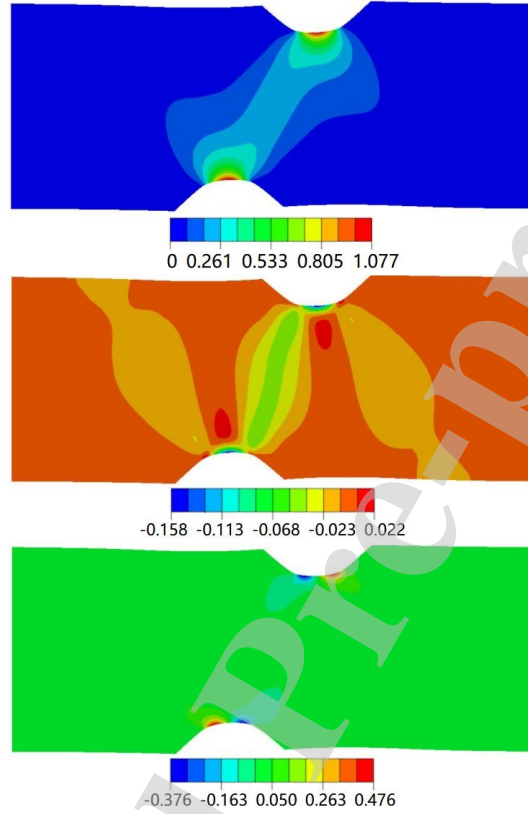


Figure 26: The strain distributions obtained by FE simulation using the identified parameters

In addition to the macroscopic material response, the simulated strain fields ε_{11} and ε_{22} (1 refers to the loading direction and 2 to the transverse direction) are shown in figure 26 and, as expected, heterogenous fields are observed.

6.4. Comments and discussion

In summary, we first identified the three Voce hardening parameters using inverse analysis, next the finite element simulations of uniaxial tension, equibiaxial tension and Meuwissen tension tests were performed with the previously identified hardening parameters. Despite the relatively straight-forward model used for the fitting, we obtain a good agreement between the numerical predictions using the identified Voce hardening parameters and experimental data.

In addition, for the equi-biaxial test, the experimentally obtained longitudinal strain distribution has been compared with the model predictions (before the onset of necking) and for different values of imposed displacements.

Conclusions

The aim of this work was to contribute to a comprehensive investigation of the anisotropic plastic deformation of pure zinc at the macroscopic scale. In the experimental portion, a variety of mechanical tests were carried out on sheet metal specimens, including uniaxial/biaxial tension, shear and Meuwisen tests along the rolling and transverse directions, to experimentally investigate the plastic anisotropy. The main findings were : similar work-hardening at higher plastic strains under monotonic loading, very low values of the Lankford coefficients despite the high ductility, and a prominent Bauschinger effect and residual ductility seen during reverse loading, that strongly depend on the forward shear direction and strain amount in forward loading. The Meuwissen tests also revealed that the force-displacement curve and maximum ductility are both very sensitive to the in-plane anisotropy. This was followed by FE modeling to simulate the plastic anisotropic behavior for various mechanical tests using classical macroscopic phenomenological anisotropic yield and hardening models, for the characterization portion. The characterization was done in two stages: first identifying the yield parameters, and next identifying the Voce isotropic hardening parameters using the FE simulations. All constitutive parameters were identified solely from the three uniaxial tensile tests, however, they were still able to give reasonably good agreement between the experimental and simulated results for all the other mechanical tests, indicating the efficacy of the approach for highly anisotropic materials, despite its ease of application.

It is clear that highly anisotropic materials need better-adapted constitutive models with significantly more attention to determining the associated model parameters. Since one could conceivably predict completely different yield parameters and Lankford coefficients despite fitting a single experimental test to

the simulated result, the characterization would require sufficient data to correctly identify the material model for accurate FE modeling of such materials. Simple mechanical tests are obviously limited in the amount of data they could generate. One "work around" would be using multi-scale VPSC type models as in our previous work [25], where the initial crystallographic texture was considered with SEM investigation and multi-scale modeling to better understand the physical mechanisms behind the macroscopic anisotropic behavior. This approach does not, in the authors opinion, appear to be justified save for very specific applications. As an example, the VPSC approach has been applied in the literature to Titanium alloys [46, 47], which are widely used in aerospace applications.

A second approach would be using a battery of experimental tests, including equi-biaxial loading in tension/compression, to generate a massive set of data for the inverse analysis. This is also understandably impractical since it would be time consuming. A third more realistic option would include "heterogenous" tests (like the Meuwissen) that attempt to capture the multi-directional plastic behaviour in a single test. This test would then be used alongside a complex model (like Cazacu) in an inverse analysis between the experimental and FE simulated strain fields as well as load-displacement curves.

As was pointed out by [48], more complex i.e. non-quadratic yield criteria, as well as more complex hardening relations, should be considered for hexagonal materials in future works.

Data availability

The raw/processed data required to reproduce these findings cannot be shared at this time as the data also forms part of an ongoing study.

References

- [1] C. Slunder, W. Boyd, Zinc: Its Corrosion Resistance, International Lead Zinc Research Organization, 1983.

- [2] R. Ramanauskas, R. Juškėnas, A. Kaliničenko, L. F. Garfias-Mesias, Microstructure and corrosion resistance of electrodeposited zinc alloy coatings, *Journal of Solid State Electrochemistry* 8 (6) (2004) 416–421. doi:10.1007/s10008-003-0444-2. URL <http://dx.doi.org/10.1007/s10008-003-0444-2>
- [3] C. van den Bos, H. Schnitger, X. Zhang, A. Hovestad, H. Terryn, J. de Wit, Influence of alloying elements on the corrosion resistance of rolled zinc sheet, *Corrosion Science* 48 (6) (2006) 1483 – 1499. doi:<http://dx.doi.org/10.1016/j.corsci.2005.05.028>. URL <http://www.sciencedirect.com/science/article/pii/S0010938X05001629>
- [4] T. H. Muster, W. D. Ganther, I. S. Cole, The influence of microstructure on surface phenomena: Rolled zinc, *Corrosion Science* 49 (4) (2007) 2037 – 2058.
- [5] R. Hill, A theory of the yielding and plastic flow of anisotropic metals, *Proceedings of the Royal Society of London A: Mathematical, Physical and Engineering Sciences* 193 (1033) (1948) 281–297. doi:10.1098/rspa.1948.0045.
- [6] E. Edwards, J. Washburn, Mstrain hardening of latent slip systems in zinc crystals, *Trans AIME* 200 (1954) 1239 – 1251.
- [7] R. L. Bell, R. W. Cahn, The dynamics of twinning and the interrelation of slip and twinning in zinc crystals, *Proceedings of the Royal Society* 239 (1957) 494–521. doi:10.1098/rspa.1957.0058.
- [8] P. B. Price, Nucleation and growth of twins in dislocation-free zinc crystals, *Proceedings of the Royal Society of London. Series A, Mathematical and Physical Sciences* 260 (1960) 251 – 262.
- [9] M. H. Yoo, J. R. Morris, K. M. Ho, S. R. Agnew, Nonbasal deformation modes of hcp metals and alloys: Role of dislocation source and mobility, *Metallurgical and Materials Transactions A* 33 (13) (2002) 813–822. doi:10.1007/s11661-002-1013-5.

- [10] P. G. Partridge, The crystallography and deformation modes of hexagonal close-packed metals, *Metallurgical Reviews* 12 (1) (1967) 169–194. doi:10.1179/mtlr.1967.12.1.169.
- [11] F. F. Lavrentyev, O. P. Salita, Y. G. Kazarov, *Fiz. Metl. Metalloved* 26 (1968) 348.
- [12] A. Bramley, P. Mellor, Plastic anisotropy of titanium and zinc sheets, *International Journal of Mechanical Sciences* 10 (3) (1968) 211 – 219. doi:https://doi.org/10.1016/0020-7403(68)90080-5.
- [13] D. Rogers, W. Roberts, Plastic anisotropy of titanium and zinc sheet—ii, *International Journal of Mechanical Sciences* 10 (3) (1968) 221 – 229. doi:https://doi.org/10.1016/0020-7403(68)90081-7.
- [14] M. Diot, Etude des modifications de composition d’alliages de zinc cuivre titane. conséquences sur l’aptitude au formage., Ph.D. thesis, University of Metz (France) (1996).
- [15] M. Diot, J. Fundenberger, M. Philippe, C. Esling, J. Wegria, Texture gradient in rolled zinc sheets, *Scripta Materialia* 39 (11) (1998) 1623 – 1630.
- [16] M. Diot, M. Philippe, J. Wegria, C. Esling, Addition elements and texture gradients in rolled zinc alloys, *Scripta Materialia* 40 (11) (1999) 1295 – 1303. doi:https://doi.org/10.1016/S1359-6462(99)00077-9.
- [17] S. Kataoka, M. Murakawa, T. Aizawa, H. Ike, Tribology of dry deep-drawing of various metal sheets with use of ceramics tools, *Surface and Coatings Technology* 177-178 (2004) 582 – 590, proceedings of the 30th International Conference on Metallurgical Coatings and Thin Films. doi:https://doi.org/10.1016/S0257-8972(03)00930-7.
- [18] G. Pantazopoulos, A. Sampani, Analysis of a weld failure of a rolled Zn-alloy strip - a case study, *Engineering Failure Analysis* 14 (4) (2007-06-01) 642(10).

- [19] G.Vincent, F.Zhang, J.J.Fundenberger, C.Esling, Experimental and simulation textures in an asymmetrically skin-passed zinc galvanized sheet, *Scripta Materialia* 53 (2005) 775 – 779.
- [20] L. F. d. Senna, S. L. D'Áz, L. A. Sathler, Hardness analysis and morphological characterization of copper-zinc alloys produced in pyrophosphate-based electrolytes, *Materials Research* 8 (2005) 275 – 279. doi:10.1590/S1516-14392005000300009.
- [21] Y. Jansen, R. E. Logé, M. Milesi, E. Massoni, An anisotropic stress based criterion to predict the formability and the fracture mechanism of textured zinc sheets, *Journal of Materials Processing Technology* 213 (6) (2013) 851 – 855. doi:https://doi.org/10.1016/j.jmatprotec.2012.12.006.
- [22] M. Milesi, R. E. Loge, Y. Jansen, Anisotropic mechanical behavior and formability criterion for zinc sheets, *Journal of Materials Processing Technology* 214 (12) (2014) 8. 2869–2876. doi:10.1016/j.jmatprotec.2014.06.023.
- [23] M. Milesi, R. Logé, D. P. Muñoz, Y. Jansen, P.-O. Bouchard, Accounting for material parameters scattering in rolled zinc formability, *Journal of Materials Processing Technology* 245 (2017) 134 – 148. doi:https://doi.org/10.1016/j.jmatprotec.2017.02.021.
- [24] M. Milesi, J. Lecoq, C. Pradille, L. Vitu, N. Boudeau, P.-O. Bouchard, Impact of strain rate sensitivity on the identification of the material parameters scattering and on the formability of zinc sheet, *International Journal of Material Forming* doi:10.1007/s12289-019-01479-2.
- [25] L. Cauvin, B. Raghavan, S. Bouvier, X. Wang, F. Meraghni, Multi-scale investigation of highly anisotropic zinc alloys using crystal plasticity and inverse analysis, *Materials Science & Engineering A* 729 (27) (2018) 106 – 118. doi:https://doi.org/10.1016/j.msea.2018.05.038.
- [26] M. Philippe, F. Wagner, F. Mellab, C. Esling, J. Wegria, Modelling of texture evolution for materials of hexagonal symmetry—i. application to

- zinc alloys, *Acta Metallurgica et Materialia* 42 (1) (1994) 239 – 250.
doi:[http://dx.doi.org/10.1016/0956-7151\(94\)90066-3](http://dx.doi.org/10.1016/0956-7151(94)90066-3).
- [27] J. Fundenberger, M. Philippe, F. Wagner, C. Esling, Modelling and prediction of mechanical properties for materials with hexagonal symmetry (zinc, titanium and zirconium alloys), *Acta Materialia* 45 (10) (1997) 4041 – 4055. doi:[10.1016/S1359-6454\(97\)00099-2](https://doi.org/10.1016/S1359-6454(97)00099-2).
- [28] F. Zhang, G. Vincent, Y. Sha, L. Zuo, J. Fundenberger, C. Esling, Experimental and simulation textures in an asymmetrically rolled zinc alloy sheet, *Scripta Materialia* 50 (7) (2004) 1011 – 1015. doi:<http://dx.doi.org/10.1016/j.scriptamat.2003.12.031>.
- [29] R. Lebensohn, C. Tome, A self-consistent anisotropic approach for the simulation of plastic deformation and texture development of polycrystals: Application to zirconium alloys, *Acta Metallurgica et Materialia* 41 (9) (1993) 2611 – 2624.
- [30] D. Lecompte, A. Smits, S. Bossuyt, H. Sol, J. Vantomme, D. V. Hemelrijck, A. Habraken, Quality assessment of speckle patterns for digital image correlation, *Optics and Lasers in Engineering* 44 (11) (2006) 1132 – 1145. doi:<https://doi.org/10.1016/j.optlaseng.2005.10.004>.
- [31] F. Meraghni, H. Nouri, N. Bourgeois, C. Czarnota, P. Lory, Parameters identification of fatigue damage model for short glass fiber reinforced polyamide (pa6-gf30) using digital image correlation, *Procedia Engineering* 10 (Supplement C) (2011) 2110 – 2116, 11th International Conference on the Mechanical Behavior of Materials (ICM11). doi:[10.1016/j.proeng.2011.04.349](https://doi.org/10.1016/j.proeng.2011.04.349).
- [32] F. Meraghni, Y. Chemisky, B. Piotrowski, R. Echchorfi, N. Bourgeois, E. Patoor, Parameter identification of a thermodynamic model for superelastic shape memory alloys using analytical calculation of the sensitivity matrix, *European Journal of Mechanics - A/Solids* 45 (2014) 226–237. doi:[10.1016/j.euromechsol.2013.12.010](https://doi.org/10.1016/j.euromechsol.2013.12.010).

- [33] E. Rauch, Plastic anisotropy of sheet metals determined by simple shear tests, *Materials Science and Engineering: A* 241 (1) (1998) 179 – 183. doi:[https://doi.org/10.1016/S0921-5093\(97\)00486-3](https://doi.org/10.1016/S0921-5093(97)00486-3).
- [34] S. Bouvier, B. Gardey, H. Haddadi, C. Teodosiu, Characterization of the strain-induced plastic anisotropy of rolled sheets by using sequences of simple shear and uniaxial tensile tests, *Journal of Materials Processing Technology* 174 (1) (2006) 115 – 126. doi:<https://doi.org/10.1016/j.jmatprotec.2005.04.086>.
- [35] S. Bouvier, H. Haddadi, P. Levée, C. Teodosiu, Simple shear tests: Experimental techniques and characterization of the plastic anisotropy of rolled sheets at large strains, *Journal of Materials Processing Technology* 172 (1) (2006) 96 – 103. doi:<https://doi.org/10.1016/j.jmatprotec.2005.09.003>.
- [36] M. Meuwissen, C. Oomens, F. Baaijens, R. Petterson, J. Janssen, Determination of the elasto-plastic properties of aluminium using a mixed numerical–experimental method, *Journal of Materials Processing Technology* 75 (1–3) (1998) 204 – 211.
- [37] Y. Chemisky, F. Meraghni, N. Bourgeois, S. Cornell, R. Echchorfi, E. Paator, Analysis of the deformation paths and thermomechanical parameter identification of a shape memory alloy using digital image correlation over heterogeneous tests, *International Journal of Mechanical Sciences* 96-97 (2015) 13–24. doi:[10.1016/j.ijmecsci.2015.03.007](https://doi.org/10.1016/j.ijmecsci.2015.03.007).
- [38] S. Bouvier, N. Benmhenni, W. Tirry, F. Gregory, M. Nixon, O. Cazacu, L. Rabet, Hardening in relation with microstructure evolution of high purity α -titanium deformed under monotonic and cyclic simple shear loadings at room temperature, *Materials Science and Engineering: A* 535 (2012) 12 – 21. doi:<https://doi.org/10.1016/j.msea.2011.12.033>.
- [39] O. Cazacu, F. Barlat, Generalization of drucker’s yield criterion to orthotropy, *Mathematics and Mechanics of Solids* 6 (6) (2001) 613–630. doi:[10.1177/108128650100600603](https://doi.org/10.1177/108128650100600603).

- [40] C. Butcher, A. Abedini, Shear confusion: Identification of the appropriate equivalent strain in simple shear using the logarithmic strain measure, *International Journal of Mechanical Sciences* 134 (2017) 273–283. doi:10.1016/j.ijmecsci.2017.10.005.
- [41] A. Abedini, C. Butcher, M. Nemcko, S. Kurukuri, M. Worswick, Constitutive characterization of a rare-earth magnesium alloy sheet (zek100-o) in shear loading: Studies of anisotropy and rate sensitivity, *International Journal of Mechanical Sciences* 128-129 (2017) 54–69. doi:10.1016/j.ijmecsci.2017.04.013.
- [42] A. Abedini, C. Butcher, T. Rahmaan, M. Worswick, Evaluation and calibration of anisotropic yield criteria in shear loading: Constraints to eliminate numerical artefacts, *International Journal of Solids and Structures* 151 (2018) 118–134. doi:10.1016/j.ijsolstr.2017.06.029.
- [43] D. C. Drucker, Relation of experiments to mathematical theories of plasticity, *Journal of Applied Mechanics* 16 (1949) 349 – 357.
- [44] B. Chaparro, J. Alves, L. Menezes, I. Fernandes, Optimization of the phenomenological constitutive models parameters using genetic algorithms, Springer, Berlin, Heidelberg, 2007, Ch. In: *Advanced Methods in Material Forming.*, pp. 35–54.
- [45] M. E. Nixon, O. Cazacu, R. A. Lebensohn, Anisotropic response of high-purity α -titanium: Experimental characterization and constitutive modeling, *International Journal of Plasticity* 26 (4) (2010) 516 – 532. doi:https://doi.org/10.1016/j.ijplas.2009.08.007.
- [46] M. Knezevic, R. A. Lebensohn, O. Cazacu, B. Revil-Baudard, G. Proust, S. C. Vogel, M. E. Nixon, Modeling bending of α -titanium with embedded polycrystal plasticity in implicit finite elements, *Materials Science and Engineering: A* 564 (2013) 116–126. doi:10.1016/j.msea.2012.11.037.

- [47] B. Morrow, R. Lebensohn, C. Trujillo, D. Martinez, F. Addessio, C. Bronkhorst, T. Lookman, E. Cerreta, Characterization and modeling of mechanical behavior of single crystal titanium deformed by split-hopkinson pressure bar, *International Journal of Plasticity* 82 (2016) 225–240. doi:10.1016/j.ijplas.2016.03.006.
- [48] W. F. Hosford, Reflections on the dependence of plastic anisotropy on texture, *Materials Science and Engineering: A* 257 (1) (1998) 1 – 8. doi:https://doi.org/10.1016/S0921-5093(98)00819-3.

HIGHLIGHTS

- Experimental investigation of the plastic anisotropy of the Zinc.
- Uniaxial/biaxial tension, shear and Meuwisen tests on sheet metal specimens.
- Identifications of anisotropic Hill criterion and Cazacu and Barlat criterion.
- Confrontation between experimental results and finite element simulations.

AUTHORSHIP STATEMENT

Manuscript title: Investigating the plastic anisotropy and hardening behavior of a commercial Zn-Cu-Ti alloy: experimental & modeling approach.

All persons who meet authorship criteria are given as follow: Ludovic Cauvin, Balaji Raghavan, Jianqiang Jin, Salima Bouvier, Xiaodong Wang, Fodil Meraghni, José Luis Alves.

All authors certify that they have participated sufficiently in the work to take public responsibility for the content, including participation in the concept, design, analysis, writing, or revision of the manuscript. Furthermore, each author certifies that this material or similar material has not been and will not be submitted to or published in any other publication before its appearance in *Mechanics of Materials*.

The authors

Declaration of interests

The authors declare that they have no known competing financial interests or personal relationships that could have appeared to influence the work reported in this paper.

The authors declare the following financial interests/personal relationships which may be considered as potential competing interests:

Journal Pre-proof